

A Low Power 100MΩ CMOS Front-End Transimpedance Amplifier for Biosensing Applications

Jiaping Hu

Department of Electrical and
Computer Engineering
Northeastern University
Boston, Massachusetts
jhu@ece.neu.edu

Yong-Bin Kim

Department of Electrical and
Computer Engineering
Northeastern University
Boston, Massachusetts
ybk@ece.neu.edu

Joseph Ayers

Department of Biology and
Marine Science Center
Northeastern University
Nahant, Massachusetts
lobster@neu.edu

Abstract—In this paper, the design, implementation and simulation of a high-gain, low-power, low-noise CMOS front-end transimpedance amplifier (TIA) is presented for interfacing with a bio-sensor array and analog neural circuits. An improved capacitive-feedback TIA topology is used with an active load to obtain a 100MΩ transimpedance gain, 1MHz bandwidth, 158fA/rt(Hz) input-referred current noise at sensing frequency, near 0° phase shift and 1V peak-to-peak output swing. The proposed circuit dissipates 132μW from a 1.8V supply and the circuit is implemented in a standard 0.18μm CMOS 1P6M technology.

I. INTRODUCTION

Recent advances in biomimetics, such as modeling based on elements of the stomatogastric ganglion and its electronic implementation, suggested a new approach to building a true autonomous biohybrid robots [1]. Due to the stringent power, area and robustness requirements in such applications, the integrated circuit approach becomes essential to the realization of biohybrid robots.

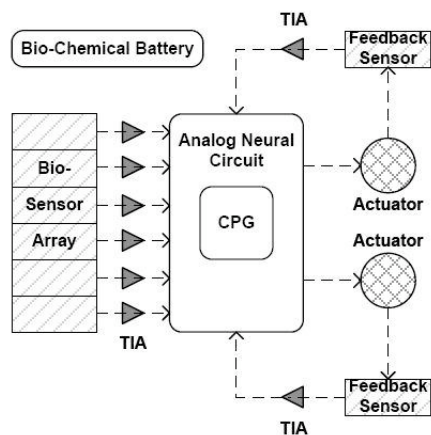


Figure 1. Block diagram of a biohybrid robot consists of: a front-end biosensor array, analog neural circuit with CPG, actuators followed by synthetic muscle, a back-end feedback biosensor, and a transimpedance amplifier in the optical-signal path. A bio-chemical battery provides power for the system.

Prior research has shown that Central Pattern Generation (CPG) is an intrinsic mechanism of an animals' natural behavior. It acts inherently as a bio-oscillator to provide neural signal throughout the network. Thus an electronic neuron-based CPG module is the core of the behavior control circuit in a neural circuit system. At the same time, a biosensor array serves as the interfacing between the external environment, CPG, actuators, and the bio-feedback generators.

One of the promising implementation methods for a biohybrid robot control system consists of biosensors, ultra-low power A/D converters, and a digital-domain processor [2]. The two main disadvantages of these digital IC solutions are its inherently discrete-time and deterministic control. On the other side, an analog electronic implementation without the need for data converters and a FSM provide the desired ability of continuous-time and adaptive control [3]. However, the latter topology also introduces design challenges in the form of trade-offs between noise, power dissipation, speed, and process variations. Figure 1 shows the block diagram of a proposed biohybrid robot system.

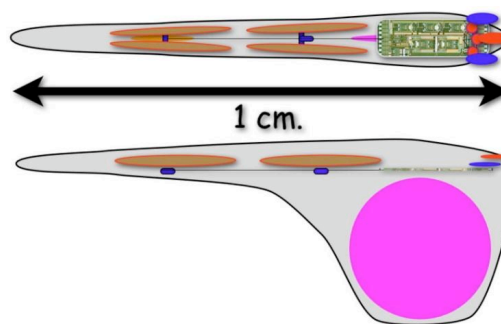


Figure 2. Sea Lamprey-based Biohybrid Robot 'Cyberplasm'[1]

The proposed biohybrid underwater robot "Cyberplasm," contains an analog electronic nervous system shown in Fig.2. A novel optical-communication mechanism is adopted to propagate and feedback control signals among blocks. Photo-diodes with a particular peak sensing wavelength are

integrated in the front-end biosensors generating signals for the following stage(s). The amplitude of the current signal is constrained to the level of nanoamps [4] due to low-power operation and low quantum efficiency of silicon, while the frequency of the signal is at kilohertz-level due to the limited sampling ability of the biosensor array. A low-noise, low-power, and high gain TIA is thus desirable in the signal path. Moreover, since the TIA works as a preamplifier for the level-sensitive analog neural circuit, its output swing should be high. At the same time, the biohybrid robot neural system also requires an in-phase operation to obtain real-time autonomous controllability. Although the sensing frequency of the biosensor arrays in our system is around 20kHz, the frequency response of the TIA should be well beyond the bio-oscillation frequency of CPG in order to reduce its phase noise [6]. In this paper, we present a novel front-end TIA design that provides a high gain, low input-referred current noise, high output swing, and proper flat phase response up to 100kHz in a standard CMOS process for a biosensing application.

This paper is organized as follows: Section II introduces and analyzes the topology used in the design. Simulation results are presented in Section III. Section IV covers the performance of the TIA and contains a comparison with prior arts.

II. CIRCUIT IMPLEMENTATION

A. Improved Capacitive-Feedback TIA

The most commonly used topology of a TIA applies a resistive-feedback mechanism, as shown in Fig.3(a). The feedback resistor R_F with a parallel C_F (not shown in the figure) sets the gain and frequency response. Another popular topology harnesses a capacitive feedback loop only, which eliminates the noise contribution from R_F . The improved TIA topology used in our low noise, high gain biosensor application is shown in Fig.3(c). First demonstrated in [5], it exhibits several advantages for our continuous biohybrid robot control application over the commonly used resistive method shown in Fig.3(a) or capacitive-feedback TIAs shown in Fig.3(b).

First, the capacitive-feedback current amplifier in Fig.3(c) drives current to the high impedance output with a gain of $(1+C_2/C_1)$. Meanwhile, the resulting large transimpedance gain of $(1+C_2/C_1) \cdot R_d$, which in turn, reduces the input-referred current noise due to the load R_d by the same factor [5,6] as shown in (2), where ω is frequency, k is the Boltzmann constant, T is temperature and v_N^2 is the amplifier input-referred voltage noise. Comparing with the resistive-feedback TIA, the proposed topology alleviates the trade-off between noise and gain.

$$\text{Gain} = R_d \cdot \left(1 + \frac{C_2}{C_1}\right) \quad (1)$$

$$i_N^2 = \frac{4kT}{R_D \left(1 + \frac{C_2}{C_1}\right)^2} + v_N^2 \omega^2 (C_1 + C_{par})^2 \quad (2)$$

Second, comparing with the common capacitive-feedback TIAs shown in Fig.3(b), the OTA in the feedback loop adds an additional 180° phase shift to the improved topology in Fig.3(c), thus avoiding the nonzero phase-response seen in Fig.3(b). It also pushes the location of the pole from large C_2

away by a factor of $(1+A_0)$ as shown in (3) [5], where gm_2 is the transconductance of transistor M2 and A_0 is the DC gain of the OTA. The equation also implies the possibility of increasing bandwidth by increasing the gain of the OTA in the new topology without reducing R_d and the transimpedance gain.

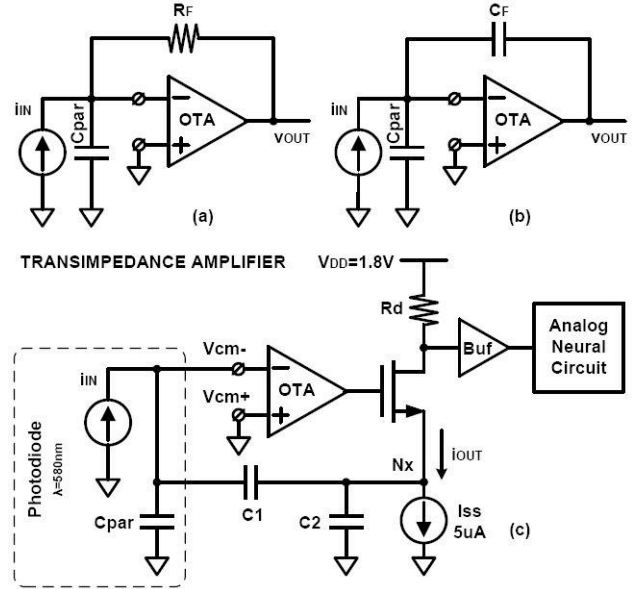


Figure 3. (a) Resistive feedback TIA; (b) Capacitive feedback TIA; (c) The schematic of the proposed TIA design with the improved capacitive feedback single-ended topology

As a result, the adopted topology relaxes the trade-offs between gain, noise and bandwidth in the desired transimpedance amplifier design. However, the noise and bandwidth of this improved capacitive feedback topology will be affected by the parasitic of the photodiode, as shown in (2) and (3). This is because a high ratio between C_2 and C_1 is desirable in our topology and hence the capacitance of C_1 will be comparable to the parasitic.

$$BW_{TIA} = \frac{gm_2(1+A_0)C_1}{C_2(C_1+C_{par})} \quad (3)$$

Since the problem from feed-through capacitance is not serious in the desired system, a single-ended structure is used for saving power and transistor/pin count. For further power reduction, transistors in the proposed TIA operate in the weak inversion region. Meanwhile, the load R_d of the TIA is implemented using a long-channel PMOS transistor to maximize the transimpedance gain. Finally, the TIA is followed by a buffer stage for driving the subsequent analog neural circuits.

B. Miller 2-Stage OPAMP

A Miller 2-Stage OPAMP with high gain, suitable GBW and low-power is designed for the capacitive feedback loop of the proposed TIA. The circuit schematic of the proposed Miller 2-stage OPAMP is shown in Figure 4.

In the input stage, large-sized PMOS transistors (35um/5um) are used to minimize the input-referred flicker noise and mismatch. Meanwhile, the large transconductance of this stage (85uS) reduces the noise contribution of the other

transistors [7]. Finally, to achieve a 1MHz bandwidth for the entire TIA, a large GBW ($>7\text{MHz}$) of the OTA is preferred. This gives an overall flat frequency-response for the TIA.

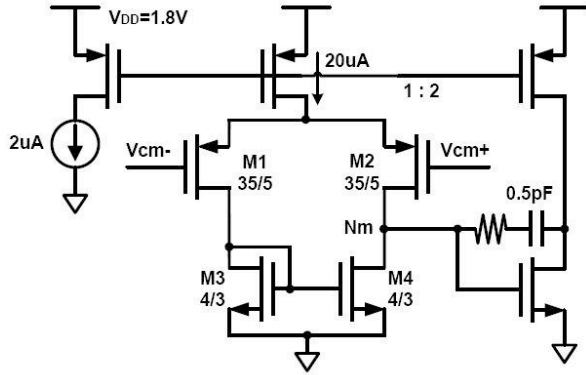


Figure 4. Schematic of the proposed miller two-stage OPAMP

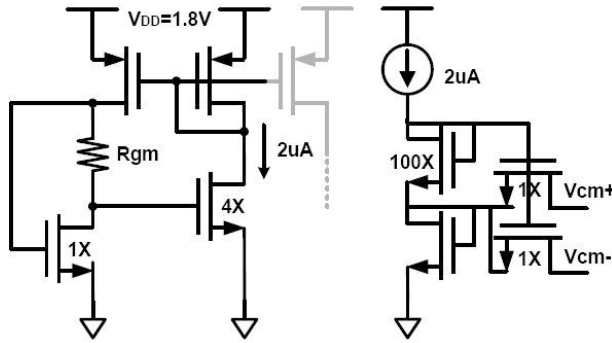


Figure 5. Schematic of the weak inversion biasing circuit

In the output stage, the values of the miller capacitor and its series resistor are chosen for an optimized stability and RHP-zero cancelling. Transistors in the current mirrors throughout the OPAMP are biased with large V_{GS} to minimize device mismatch and noise. Non-minimal sized transistors are also used to improve the gain and mismatch. However, attention needs to be paid to the resulting increased C_{GD} and C_{GS} at high impedance node (N_m). Moreover, the body and source terminals of the PMOS transistors are connected together in the circuit, which is achievable in typical n-well processes to reduce the potential hot-carrier effect. Table I summarized the simulated characteristics of the OPAMP.

TABLE I. SUMMARY OF THE SIMULATED OPAMP PERFORMANCE

Parameter	Measured Value
Technology	0.18 μm CMOS
DC Gain	103dB
Unity GBW	20MHz
Phase Margin	63 $^\circ$
Noise Floor	25nV/rt(Hz)
Power Dissipation	110 μW
Power Supply	1.8V

Figure 5 shows the schematic of the biasing circuits used in the design [5]. In order to improve the low-frequency stability of the amplifier, long-channel devices are used to boost the on-resistance of the transistors in the voltage biasing circuit and to improve mismatch in the constant-gm current biasing circuit. As a result, the common-mode voltage is delivered to the input nodes through a 2.5M Ω resistor, and the TIA achieves a 40Hz low cut-off frequency.

III. SIMULATION RESULTS

Simulation results for the AC analysis are shown in Fig.6. The proposed TIA exhibits a 100M Ω transimpedance gain, which not only ensures the functionality of the level-sensitive analog neural circuit, but also relaxes the noise requirement of the system.

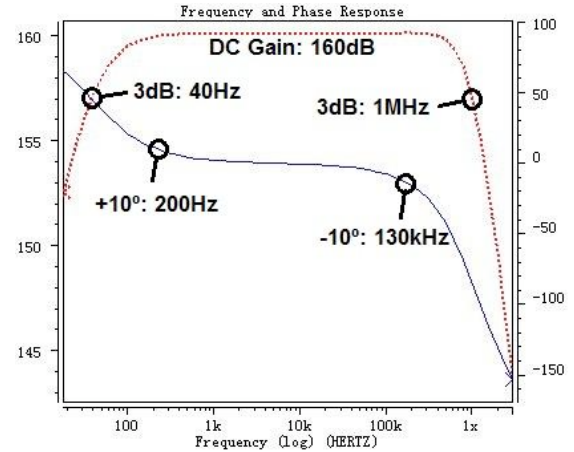


Figure 6. AC performance of the proposed TIA. Y-Axis Left: Transimpedance Gain in dB Ω (dot-line); Y-Axis Right: Phase Response in degrees (line)

Meanwhile, it keeps a flat frequency-response up to 1MHz, which is suitable for controlling the proposed underwater biohybrid robot. Moreover, the TIA shows a phase-response within 10 $^\circ$ from 200Hz to 130 KHz, thus the in-phase control of the system for our biosensing (20kHz) and oscillating (100kHz) application is achieved. Input-referred current noise, shown in Fig.7, is kept under 200fA/rt(Hz) at the sensing frequency of 20kHz. Meanwhile the flicker noise corner is located under 20Hz. Thus the desired low-noise performance of the front-end TIA at sensing frequency is assured.

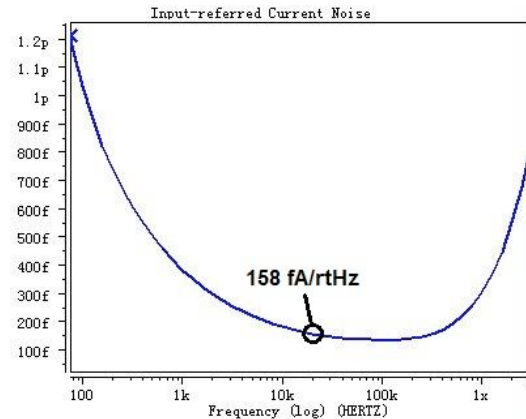


Figure 7. Input-referred current noise at sensing frequency in A/rt(Hz)

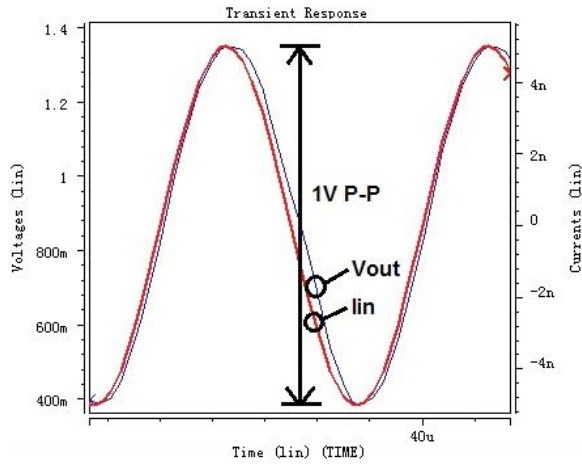


Figure 8. Maximum output voltage swing of the TIA. Y-Axis Left: Output Voltage in volts; Y-Axis Right: Input Current in amperes.

The transient performance is also measured at the practical operating frequency of the biohybrid robot control circuit. The TIA exhibits a $\sim 1V$ peak-to-peak output voltage swing, as shown in Fig.8. The in-phase signal amplification of the circuit is also observed from this transient analysis.

TABLE II. POWER DISSIPATION OF THE TIA

Block	Power
OPAMP	110 μ W
Biasing	11 μ W
Output Stage	11 μ W
Total	132 μ W

Finally, the power dissipation of the TIA is measured and summarized in Table II. The high performance OPAMP in the feedback loop introduces a new set of design trade-offs among transimpedance gain, bandwidth and power, thus providing the flexibility for further modification.

IV. SUMMARY

The proposed design achieves 100M Ω transimpedance gain, 1MHz 3dB-Bandwidth, and $\pm 10^\circ$ phase shift between 0.2-130kHz. With an additional flexibility in design trade-offs between gain and BW, the AC performance of the proposed TIA is suitable for biosensing applications. Low current consumption (73 μ A) as well as low input-referred current noise (158fA/rt(Hz)) are both obtained in the design. Finally, a 1V peak-to-peak output voltage swing is measured. This allows the easy integration of the design into the proposed autonomous underwater biohybrid robots control system.

Table III shows a comparison of this design with prior arts. The topology of the proposed design was first demonstrated in [5]. TIAs in the second and third column were designed for MEMS applications, which have a very similar set of design

specifications as the biosensing applications in the last two columns. The proposed design achieves the highest transimpedance gain and lowest power consumption with comparable bandwidth and noise.

TABLE III. TABLE III. COMPARISON WITH PRIOR ARTS

Parameter	[5]	[6]	[8]	[9]	This work
Application	Receiver	MEMS	MEMS	Biosensor	Biosensor
Technology	.6 μ m CMOS	.18 μ m CMOS	.6 μ m CMOS	.35 μ m CMOS	.18 μ m CMOS
DC Gain	8.7k Ω	56M Ω	1.6M Ω	65M Ω	100M Ω
Bandwidth	550MHz	1.8 MHz	230 KHz	2 MHz	1 MHz
Cutoff Freq	50 kHz	<5kHz	<1Hz	100Hz	40Hz
Input noise	4.5pA/rtHz	65fA/rtHz	88fA/rtHz	3fA/rtHz	158fA/rtHz
Power	30mW	436 μ W	400 μ W	25mW	132 μ W

V. CONCLUSION

This paper describes a transimpedance amplifier for biosensors. It utilizes an improved capacitive-feedback topology to avoid the design issue stemming from large on-chip resistors and increase the design flexibility in gain-bandwidth trade-off. The proposed TIA is implemented in a standard TSMC 0.18 μ m technology. The design demonstrates a 100M Ω transimpedance gain with 1MHz bandwidth, less than 10° phase shift between 0.2-130kHz, 1V Peak-to-Peak voltage swing, 158fA/rt(Hz) input-referred current noise at the biosensors sampling frequency, while dissipating 132 μ W power from a 1.8V supply.

REFERENCES

- [1] Ayers, J. and N. Rulkov (2007). *Controlling Biomimetic Underwater Robots with Electronic Nervous Systems*. In: *Bio-mechanisms of Animals in Swimming and Flying*, Springer-Verlag. Pp. 295-306.
- [2] Shuenn-Yuh Lee ; Chih-Jen Cheng ; Cheng-Pin Wang ; Shyh-Chyang Lee. "A 1V 8Bit 0.95mW Successive Approximation ADC for Biosignal Acquisition Systems", ISCAS 2009. IEEE.
- [3] J. Lee, Y. J. Lee, K. Kim, Y. B. Kim, and J. Ayers (2007) "Low Power CMOS Adaptive Electronic Central Pattern Generator Design for a Biomimetic Robot", *Neurocomputing* 71: 284-296.
- [4] Indal Song, "Multi-Gbit/s CMOS Transimpedance Amplifier with Integrated Photodetector for Optical Interconnects", PhD Thesis.
- [5] B. Razavi, "A 622Mb/s 4.5pA/rtHz CMOS Transimpedance Amplifier", *ISSCC Tech. Digest*, San Francisco, CA, Feb. 7-9, 2000, pp. 162-163.
- [6] James Salvia, Pedram Lajevardi, Mohammad Hekmat, and Boris Murmann, "A 56M Ω CMOS TIA for MEMS Applications", *Custom Integrated Circuits Conference* 2009.
- [7] P.R.Gray,R.G.Meyer,P.J.Hurst,andS.H.Lewis, *Analysis and Design of Analog Integrated Circuits*. Hoboken, NJ, Wiley, 2001.
- [8] A. Sharma, M.F. Zaman, F. Ayazi, "A 104-dB dynamic range transimpedance-based CMOS ASIC for tuning fork microgyroscopes", *JSSC*, vol. 42, no. 8, Aug. 2007, pp. 1790-1802.
- [9] G. Ferrari, F. Gozzini, M. Sampietro, "A current-sensitive front-end amplifier for nano-biosensors with a 2MHz BW", *ISSCC Dig. Tech. Papers*, pp. 164-165, Feb. 2007.